Characterization of Thermal Transport in Carbon Nanotube Yarns

J. L. Wang[1,*], S. S. He[2], J. J. Bao[1], X. Zhang[3], J. K. Yang[1] and Y. F. Chen[1]

[1]School of Mechanical Engineering and Jiangsu Key Laboratory for Design and Manufacture of Micro/Nano Biomedical Instruments, Southeast University, Nanjing 210096, PR China

[2]Key Laboratory of Advanced Ceramics and Machining Technology, Ministry of Education, School of Material Science and Engineering, Tianjin University, Tianjin 300072, PR China

[3]Department of Engineering Mechanics, Key Laboratory for Thermal Science and Power Engineering of Education Ministry, Tsinghua University, Beijing 100084, PR China

ABSTRACT

The carbon nanotube yarns (CNTYs) are directly spun from an aerogel form in a chemical vapor deposition reactor. The as-spun CNTYs are subjected to different post-processes, such as nitric acid treatment, twisting, and doping with iodine. The defect concentrations are detected by Raman spectroscopy, and the effective thermal conductivity is measured by a T-type probe. The results show that, the lattice thermal conductance per unit length decreases smoothly with increasing defects induced by acid treatment and iodine-doping. The twisted yarn introduces moderate defect, but an abnormal decrease in the lattice thermal conductance per unit length is observed as the twist angle increases to ~70°, indicating the phonon-soften phenomenon when CNT is subjected to the torsion stress. The effective thermal conductivity is found to increase linearly as porosity decreases, however, it is still an open question if the linear relationship holds true for highly densified CNTYs.

1. INTRODUCTION

Carbon nanotube (CNT) has been attracting lots of attentions due to its outstanding mechanical, electronic and optical properties [1]. Most potential applications require the development of macroscopic assemblies of CNTs, such as CNT mats [2] , CNT composite films [3, 4], CNT nanofluids [5], aligned CNT sheets [6] and etc. Among these, the CNT yarns (CNTYs), which consist of aligned and interconnected CNTs, are promising for lightweight, thermally and electrically conductive materials [7].

Significant effects have been made to investigate the mechanical and electrical properties of CNTYs, comparatively, the reports on the thermal transport are limited [8]. The effective thermal conductivity of CNTYs depends on microscopic structures, such as defect, tube-tube contact, alignment, density and etc [9-17]. These features are sometimes related with each other. For instance, nitric acid treatment, which is commonly used to purify CNTYs, not only shrinks diameter, but also generates additional defects in the CNT network [18]. Therefore, it is challenging to evaluate each effect separately on the thermal property of CNTYs, and the thermal transport in CNTYs is not well understood. In the case of packing density, to compare the effective thermal conductivity of CNTYs at different densities, the measured value was adjusted by using the simply mixing law, which assumes that the production of effective thermal conductivity and density is constant [11, 15, 16]. Additionally, the relative importance of thermal transport by intrinsic conductivity and contact resistance between CNTs on the effective thermal conductivity of CNTYs is still debatable [2, 19].

To find the relationship between the effective thermal conductivity and porosity of CNTYs, in this work, we changed the porosity of the as-spun CNTYs by three different post-processes, such as nitric acid treatment, twisting, and doping by iodine (I). The effective thermal conductivity was measured by the T-type probe method at room temperature, and the effects of defect scattering and porosity were separately discussed.

*Corresponding Author: wangjianli@seu.edu.cn

2. EXPERIMENTAL

2.1. Sample preparation

The CNTYs used for the experiments were spun from an aerogel form in a chemical vapor deposition (CVD) reactor [20]. Figure 1 shows the scanning electron microscopy (SEM) images of the samples. The CNTYs, consisting of double-walled carbon nanotubes (DWCNTs), have an average diameter of about 160 μm (Figure 1a). DWCNTs have coalesced into bundles, which are aligned and interconnected (Figure 2a). Most of DWCNTs exhibit a ribbon-like morphology with an equivalent diameter of about 4 nm, as seen in Figures 2(b-c). The packing density was measured to be about 0.05 g cm^{-3} by the weight and cross-sectional area of CNTYs. The acid treated CNTYs (S/CNTYs) were obtained by immersing the as-spun CNTYs into an aqueous solution of concentrated nitric acid (65 wt.%) at 100°C for 5 h, then washed by using distilled water several times to remove the residual acid. The diameter of S/CNTY decreases to about 40 μm due to the surface tension of solvents, meanwhile, the CNT bundles are coarsened (Figure 2d) compared with the raw yarns. The transmission electron microscopy (TEM) image shows that the bundle and inter-bundle spacing is free of iron catalyst as existed in the as-spun yarns (Figure 2e), which can be also verified by the energy dispersive X-ray (EDX) spectroscopy (Table 1). To obtain the I-doped CNTYs (I/CNTYs), the raw yarns were placed in the iodine vapor at 180°C for 24 h. The I/CNTYs have the similar diameter as the as-spun CNTYs, but the CNT bundles are more concentrated than those in raw yarns, which increase up to about 100 nm (Figure 2f). The twisted CNTYs (CNTY-Ns) were obtained with the aid from a rotated disk. During the twisting process, the as-spun CNTY was vertical to the pan as its one end was fixed. The surface twist angle is calculated to be about 70° based on the twist level (10^3 turns/m) and the fiber diameter (100 μm, Figure 1d).

2.2. Raman spectra

Raman spectra were collected using a cofocal Raman system (inVia-ReflexTM) at an excitation wavelength of 514 nm, an intensity of 10 mW, and a data acquisition time of 60s. The laser beam was focused to a spot of about 1.5 μm in diameter by a 100 × objective. As shown in Figure 2, Raman spectra of the as-spun CNTY, S/CNTY and I/CNTY are marked by two major peaks at 1358 cm^{-1} (D band) and 1590 cm^{-1} (G band). The D band and G band are both down shifted by 16 cm^{-1} after twisting, indicating the elongation of carbon-carbon bonds due to strain [21]. Meanwhile, for I/CNTY, two new bands not associated with CNTs are presented distinctly at 108 cm^{-1} and 175 cm^{-1} in the low frequency region, as observed by other works [22, 23]. The D band is related to the breathing oscillation of hexagonal carbon rings which can only occur when the symmetry is broken, and the G band is caused

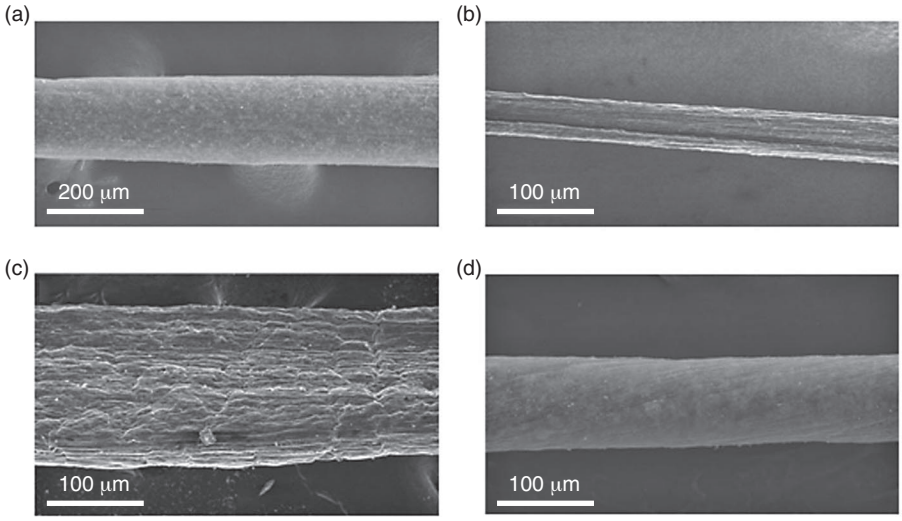

Figure 1. SEM micrographs of (a) as-spun CNTYs, (b) S/CNTYs, (c) I/CNTYs, and (d) CNTY-N

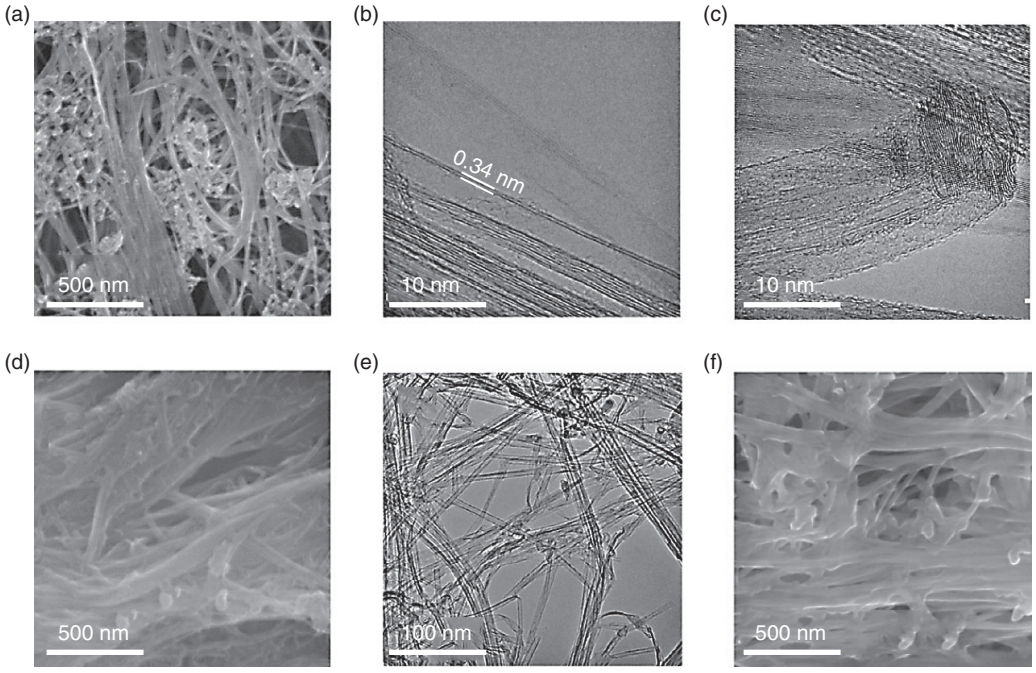

Figure 2. Morphology of the CNTYs. (a-c) SEM and HR-TEM micrographs of as-spun CNTYs, (d, e) SEM and HR-TEM micrographs of the S/CNTYs, (f) SEM images of I/CNTYs

Table 1. Elemental composition of CNTYs by EDX, unit: at.%

	I	C	O	Si	S	Fe
CNTY	–	94.26	3.49	0.20	0.39	1.66
S/CNTY	–	93.59	5.96	–	0.44	–
I/CNTY	0.62	93.78	3.73	0.34	0.21	1.32

by the stretching of the bond between the two carbon atoms, therefore, the ratio of the integrated intensities (I_D/I_G) is commonly used to quantify the defect concentration in graphitic materials. From Figure 3, an increase of the I_D/I_G value is observed in CNTF-N, S/CNTY and I/CNTY compared with that of the as-spun CNTY (I_D/I_G~0.49), indicating the different amount of disorders.

2.3. T-type probe method

The effective thermal conductivity (k_{eff}) of CNTYs in longitudinal direction was measured by the T-type probe at room temperature, and the electrical conductance (σ) was measured by the standard four-probe configuration. The experimental setup is shown in Figure 3. The CNTY was located in a homemade vacuum chamber, which was continuously evacuated by a vacuum pump and a molecular pump to obtain a vacuum level of 10^{-4} Pa. A short Pt wire (diameter 19.0 μm, length 21.0 mm) served simultaneously as a thermometer and a heater, which was subjected to a direct current. If both ends of the Pt wire were ideally heat sunk to the substrate, a parabolic temperature distribution would be formed along the Pt wire. When the free end of fiber was connected to the midpoint of the Pt wire with an interstitial material, using the same amount of Joule heating, the temperature of the Pt wire was reduced because some heat will conduct out through the test sample. Thus, measurements of the average temperature rise of the Pt wire with and without the attached CNTY allowed us to determine the total thermal resistance due to the introduction of the sample. Due to the large aspect ratio, the radiation heat loss from the CNTY surface has a large effect on the experimental results. As a consequence, the

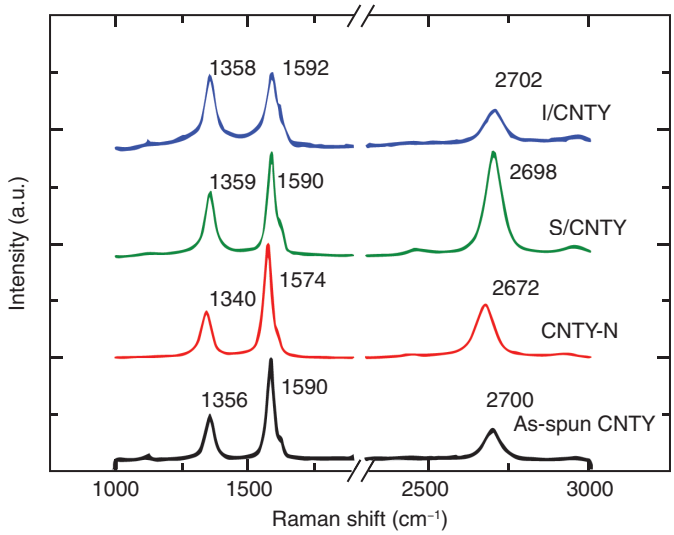

Figure 3. Raman spectra of the D band, G band and G′ band measured at a 514 nm excitation wavelength

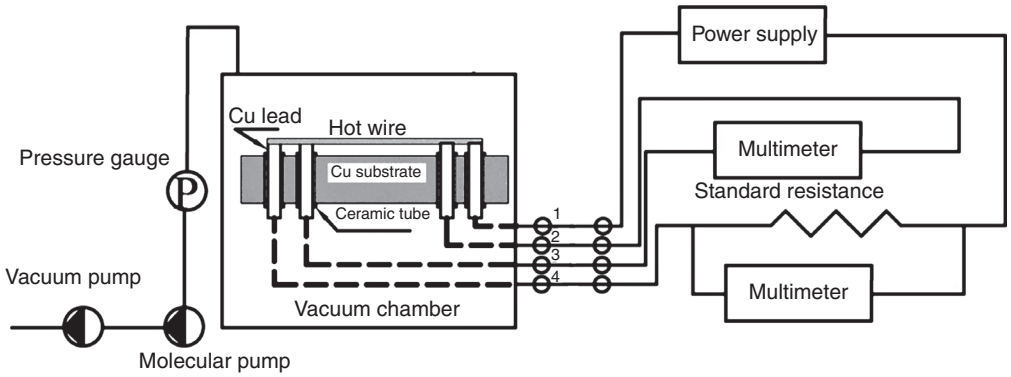

Figure 4. Measurement systems, where one end of the carbon fiber is placed at the midpoint of the hot wire

relationship between the total thermal resistance introduced by the attached CNTY and its thermal conductivity can be expressed as

$$\chi = \frac{\tanh\left(\sqrt{\pi hDR}\right)}{\sqrt{\pi hDR}} R \tag{1}$$

where D is the diameter, h is the heat transfer coefficient, calculated by $h \approx 4\varepsilon\sigma T_0^3$, with the test temperature T_0, Stefan-Boltzmann constant σ, and emissivty ε be 1, R is the thermal resistance which is defined by

$$R = \frac{l}{k_{\text{eff}} S} \tag{2}$$

with length l, cross-sectional area S. Other details can be found in previous work [24], therefore are not discussed here.

3. RESULTS AND DISCUSSION

3.1. Defects effect on thermal conductance

Table 2 shows the effective thermal conductivity and electrical conductance of CNTYs. If the thermal transport in CNTYs is considered to contribute separately from electrons and phonons, the effective thermal conductivity is calculated by $k_{\text{eff}} = k_{\text{L}} + k_e$, where k_{L} and k_{e} are lattice and electronic thermal conductivity, respectively. According to the Wiedemann-Franz Law, i.e. $k_{\text{e}} = L\sigma T$, L is the Lorenz number (2.45×10^{-8} W Ω K^{-2}), σ is the electron conductance, and T is the absolute temperature. The electronic component of thermal conductivity is less than 5%, therefore the heat transport in CNTYs is believed to be dominated by phonons. The lattice thermal conductivity is obtained by subtracting the electronic contributions from the effective thermal conductivity. To eliminate the influence from the packing density of CNTYs, we define the lattice thermal conductance as

$$G_{\text{L}} = k_{\text{L}} S/l \tag{3}$$

where l = 1 m. Note that the lattice thermal conductance at room temperature is mainly limited by tube-tube contact conductance and the intrinsic thermal conductivity of individual CNTs.

The CNT bundles in S/CNTY (Figure 2d) and I/CNTY (Figure 2f) are enlarged compared with the as-spun CNTY (Figure 2a), indicating the augmentation of the contact area among CNTs. Since the thermal contact conductance increases by two orders magnitude from the cross contact to aligned contact, the lattice thermal conductance is expected to increase due to the larger contact area. However, the lattice thermal conductance of CNTYs is found to decrease after acid treatment and doping with iodine. Therefore, it is reasonable to anticipate that the intrinsic thermal conductivity of individual CNTs dominants the thermal transport in CNTYs, which is also verified by the recent theoretical results [19].

The intrinsic thermal conductivity of CNTs can be estimated by

$$k_{\text{L}} = \frac{1}{3} C v \Lambda \tag{4}$$

where C is the specific heat, v is the phonon group velocity, and Λ is the phonon mean free path, which is limited by the phonon-phonon scattering and phonon-defect scattering. Since the samples are all post-processed from the same raw CNTYs, the specific heat is assumed to be constant among these samples. The mean free path limited by the phonon-phonon scattering which is approximately unchanged if the characteristic parameters of crystal structure [25] are assumed to have the same value for all the samples, so the lattice thermal conductance at room temperature can be used to estimate the effect of defect scattering on the thermal transport in CNTYs. The amount of defects to some extent can be characterized by the crystallite size La, and $I_{\text{D}}/I_{\text{G}}$ is correlated with La by [26]

Table 2. Thermal and electrical properties of various CNTYs

	l (mm)	D (μm)	k_{eff} (W m^{-1} K^{-1})	σ (10^3 S m^{-1})	$I_{\text{D}}/I_{\text{G}}$
As-spun CNTY	11.0 12.1	160	2.13 2.27	3.0	0.49
Twisted CNTY	12.1 12.1	160 160	2.22 1.53	– –	– –
CNTY-N	11.6 14.2	100	2.51 2.49	10.2	0.51
S/CNTY	14.2 14.2	40	29.2 28.9	72.0	0.67
I/CNTY	14.1 14.1	140	2.12 2.23	8.9	0.88

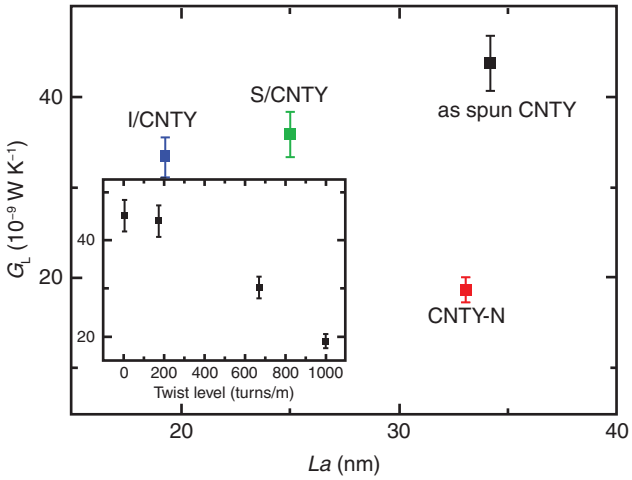

Figure 5. Lattice thermal conductance of CNTYs versus crystallite size. Inset shows the variation of lattice thermal conductance as a function of twist level

$$La = 2.4 \times 10^{-10} \lambda_{laser}{}^{4} \left(\frac{I_D}{I_G} \right)^{-1} \tag{5}$$

where λ_{laser} is the laser wavelength. As shown in Figure 5, the lattice thermal conductance of CNTYs is found to decrease smoothly as *La* increases except for CNTY-N. The possible explanations for the weakly *La*-dependent behavior are: (1) phonon-phonon scattering in CNTYs plays a significant role at room temperature, so the lattice thermal conductance is not sensitive enough to the defect variations at room temperature; (2) the impurity scattering can not be ignored, which is attributed to the catalytic agent in as-spun CNTYs and iodine inserted among CNT sheets in I/CNTYs (Table 1).

It is interesting to find that the lattice thermal conductance of CNTY-N is about two times smaller than that of the as-spun CNTYs, even though I_D/I_G remains approximately constant (Table 2). To verify the measurement accuracy, the same as-spun CNTY is manually twisted in situ in the T type probe when the solid contact between the CNTY and platinum wire is unchanged (similar procedure is presented in Ref. [24]), and the twist levels are changed to 170 and 670 turns/m, respectively. The lattice thermal conductance is found to decrease as the twist level increases. According to Eq. (4), the decrease in lattice thermal conductivity is likely to be originated from the decrease of the phonon group velocity. High twist level is believed to elongate the carbon-carbon bonds, which can be testified by the Raman spectrum (down shifts of D band and G band), thus lows the vibrational frequency. Phonon softening will reduce group velocity, and finally decreases the lattice thermal conductance. In comparison with the lattice thermal conductance, the electrical conductance increases after twisting, which is consistent with the previous work [11]. One explanation for this trend in electrical conductance is based on the fact that twisting process reduces the number of dangling tubes, thus increases the current pathway. The different tendency for thermal and electrical conductance in CNTY-N further confirms that the intrinsic thermal conductivity plays a more important role in thermal transport than the tube-tube thermal contact conductance.

3.2. Porosity dependent thermal conductivity

The effective thermal conductivity of S/CNTYs is almost 15 times larger than that of as-spun CNTYs (Table 2). As analysis above, the lattice thermal conductance decreases after acid treatment, therefore, it is anticipated that the large effective thermal conductivity is mainly attributed to the relatively low porosity of S/CNTYs.

The theoretical close-packed density (ρ_{CNT}) varies from 1.3 to 2.1 g cm^{-3} [16, 27] with different diameters of constituent CNTs. In view of the collapsed structure of carbon sheets in DWCNTs (Figure 2c), the CNT density is estimated to be 1.7 g cm^{-3} [28], so the porosity can be calculated by

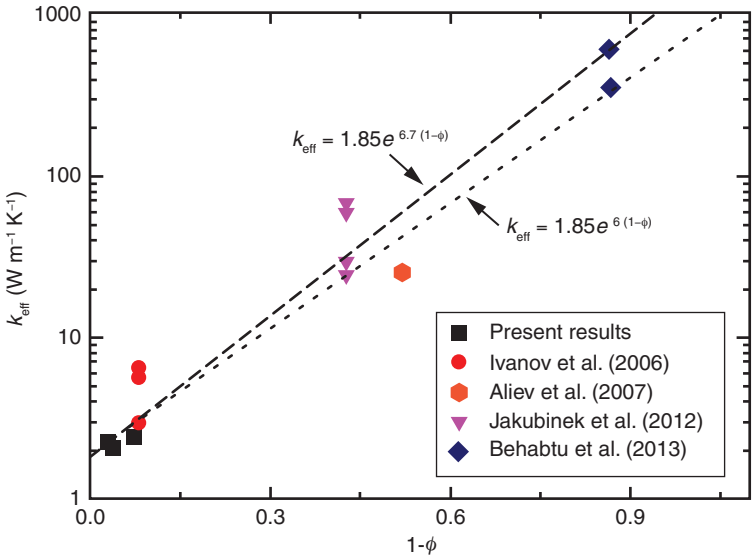

Figure 6. Effective thermal conductivity of CNTYs versus porosity

$$\phi = 1 - \frac{\rho_{CNTY}}{\rho_{CNT}} \tag{6}$$

ρ_{CNTY} is the bulk density, which was calculated by the weight of CNTYs. The porosity of the as-spun CNTYs is about 97%, and the corresponding effective thermal conductivity is about 2.2 W m^{-1} K^{-1}. If the effective thermal conductivity depends linearly on porosity, the scaled thermal conductivity of S/CNTY (porosity of about 55 %) is 35.2 W m^{-1} K^{-1}. Taking the defect scattering into consideration, the scaled value agrees reasonable well with the experimental result (28.5 W m^{-1} K^{-1} for S/CNTYs).

The effective thermal conductivity depends linearly on porosity, which holds relative good for the samples with low packing density [11, 15, 29]. However, ultrahigh thermal conductivity (over 380 W m^{-1} K^{-1}) was obtained recently when porosity is less than 10% [16], which obviously violates the linear behavior. Combined with the previous data, the effective thermal conductivity of CNTYs as a function of porosity is as shown in Figure 6. Although the qualities and structural parameters of CNTs in different groups vary with each other, the effective thermal conductivity follows an exponential, but not linear, relationship with porosity in the whole range: an abnormal increase is observed when porosity is smaller than 0.5. The experimental results are fitted by

$$k_{eff} = k_0 e^{A(1-\phi)} \tag{7}$$

with k_0 of about 1.85 W m^{-1} K^{-1} and A ranging from 6 to 6.7. In the recent review paper [29], the linear relationship between the thermal conductivity and porosity is fitted coarsely for the vertical aligned CNT films, however, it is still an open question whether the relationship holds true for low porosity samples (porosity smaller than 0.5). Due to its anisotropic heat transport, the well-known theories in porous materials, such as the percolation theory [30] and effective medium theory [31], can not be directly applied to CNTYs. The precise relationship between the porosity and thermal transport in CNTYs is not well understood, further research is needed to account for the porosity nature of CNTYs especially for the samples with porosity less than 50%.

4. CONCLUSIONS

We measured the effective thermal conductivity of S/CNTYs, I/CNTYs and CNTY-N, which were made from the same CNTYs. The lattice thermal conductance of CNTYs at room temperature is found

to decrease smoothly after acid treatment and doping with iodine, indicating that the intrinsic thermal conductivity of CNTs plays a much greater role in the thermal transport in CNTYs than the tube-tube contact conductance. After twisting, phonon group velocity decreases, leading to the decrement of the lattice thermal conductance of CNTY-N. The effective thermal conductivity increases linearly as porosity decreases for the CNTYs with low packing density, however, the thermal transport in highly densified samples is still not well understood.

ACKNOWLEDGMENTS

This work is supported by the National Basic Research Program of China (Grant No 2011CB707605), the National Natural Science Foundation of China (Grant Nos. 51476033, 51106029, 51176032, 51327001), and the Ph.D. Programs Foundation of Ministry of Education of China (Grant No. 20110092120006).

REFERENCES

[1] Dresselhaus, M. S., Dresselhaus, G., Charlier, J. C. and Hernandez, E., Electronic, thermal and mechanical properties of carbon nanotubes, *Phil. Trans. R. Soc. Lond. A*, 2004, 362, 2065–2098.

[2] Prasher, R. S., Hu, X. J., Chalopin, Y., Mingo, N., Lofgreen, K., Volz, S., Cleri, F. and Keblinski, P., Turning carbon nanotubes from exceptional heat conductors into insulators, *Phys. Rev. Lett.*, 2009, 102, 105901.

[3] Gojny, F. H., Wichmann, M. H. G., Fiedler, B., Kinloch, I. A., Bauhofer, W., Windle, A. H. and Schulte, K., Evaluation and identification of electrical and thermal conduction mechanisms in carbon nanotube/epoxy composites, *Polymer*, 2006, 47, 2036–2045.

[4] Xuan, Y. M. and Li, Q., Investigation on convective heat transfer and flow features of nanofluids, *J. Heat Transfer*, 2003, 125, 151–155.

[5] Marconnet, A. M., Yamamoto, N., Panzer, M. A., Wardle, B. L. and Goodson, K. E., Thermal conduction in aligned carbon nanotube–polymer nanocomposites with high packing density, *ACS Nano*, 2011, 5(6), 4818–4825.

[6] Hu, X. J., Padilia, A. A., Xu, J., Fisher, T. S. and Goodson, K. E., 3-omega measurements of vertically oriented carbon nanotubes on silicon, *J. Heat Transfer*, 2006, 128(11), 1109–1113.

[7] Lu, W. G., Zu, M., Byun, J. H., Kim, B. S. and Chou, T. W., State of the art of carbon nanotube fibers: opportunities and challenges, *Adv. Mater.*, 2012, 24, 1805–1833.

[8] Miao, T. T., Ma, W. G., Zhang, X., Wei, J.Q. and Sun, J. L., Significantly enhanced thermoelectric properties of ultralong double-walled carbon nanotube bundle, *Appl. Phys. Lett.*, 2013, 102, 053105.

[9] Zhou, W., Vavro, J., Guthy, C., Winey, K. I., Fischer, J. E., Ericson, L. M., Ramesh, S., Saini, R., Davis, V. A., Kittrell, C., Pasquali, M., Hauge, R. H. and Smalley, R. E., Single wall carbon nanotube fibers extruded from super-acid suspensions: preferred orientation, electrical, and thermal transport, *J. Appl. Phys.*, 2004, 95(2), 649–655.

[10] Badaire, S., Pichot, V., Zakri, C., Poulin, P., Launois, P., Vavro, J., Guthy, C., Chen, M. and Fishcher, J. E ., Correlation of properties with preferred orientation in coagulated and stretch-aligned single-wall carbon nanotubes, *J. Appl. Phys.*, 2004, 96(12), 7509–7513.

[11] Aliev, A. E., Guthy, C., Zhang, M., Fang, S., Zakhidov, A. A., Fischer, J. E. and Baughman, R. H., Thermal transport in MWCNT sheets and yarns, *Carbon*, 2007, 45, 2880–2888.

[12] Borca-Tasciuc, T., Vafaei, S., Borca-Tasciuc, D. A., Wei, B. Q., Vajtai, R. and Ajayan, P. M., Anisotropic thermal diffusivity of aligned multiwall carbon nanotube arrays, *J. Appl. Phys.*, 2005, 98, 054309.

[13] Jin, R., Zhou, Z. X., Mandrus, D., Ivanov, I. N., Eres, G., Howe, J. Y., Puretzky, A. A. and Geohegan, D. B., The effect of annealing on the electrical and thermal transport properties of macroscopic bundles of long multi-wall carbon nanotubes, *Physica B*, 2007, 388, 326–330.

[14] Kunadian, I., Andrews, R., Menguc, M. P. and Qian, D., Thermoelectric power generation using doped MWCNTs, *Carbon*, 2009, 47, 589–601.

[15] Jakubinek, M. B., White, M. A., Li, G., Jayasinghe, C., Cho, W., Schulz, M. J. and Shanov, V., Thermal and electrical conductivity of tall, vertically aligned carbon nanotube arrays, *Carbon*, 2010, 48, 3947–3952.

[16] Jakubinek, M. B., Johnson, M. B., White, M. A., Jayasinghe, C., Li, G., Cho, W., Schulz, M. J. and Shanov, V., Thermal and electrical conductivity of array-spun multi-walled carbon nanotube yarns, *Carbon*, 2012, 50, 244–248.

[17] Behabtu, N., Young, C., Tsentalovich, D. E., Kleinerman, O., Wang, X., Ma, A. W. K., Bengio, E. A., ter Waarbeek, R. F., de Jong, J. J., Hoogerwerf, R. E., Fairchild, S. B., Ferguson, J. B., Maruyama, B., Kono, J., Talmon, Y., Cohen, Y., Otto, M. J. and Pasquali, M., Strong, light, multifunctional fibers of carbon nanotubes with ultrahigh conductivity, *Science*, 2013, 339, 182–186.

[18] Monthioux, M., Smith, B. W., Burteaux, B., Claye, A., Fischer, J. E. and Luzzi, D. E., Sensitivity of single-wall carbon nanotubes to chemical processing and electron microscopy investigation, *Carbon*, 2001, 39, 1251–1272.

[19] Volkov, A. N. and Zhigilei, L. V., Heat conduction in carbon nanotube materials: strong effect of intrinsic thermal conductivity of carbon nanotubes, *Appl. Phys. Lett.*, 2012, 101, 043113.

[20] Zhong, X. H., Li, Y. L., Liu, Y. K., Qiao, X. H., Feng, Y., Liang, J., Jin, J., Zhu, L., Hou, F. and Li, J. Y., Continuous multilayered carbon nanotube yarns, *Adv. Mater.*, 2010, 22(6), 692–696.

[21] Cronin, S. B., Swan, A. K., Unlu, M. S., Goldberg, B. B., Dresselhaus, M. S. and Tinkham, M., Measuring the uniaxial strain of individual single-wall carbon nanotubes: resonance Raman spectra of atomic-force-microscope modified single-wall nanotubes, *Phys. Rev. Lett.*, 2004, 93(16), 167401.

[22] Rauf, H., Pichler, T., Pfeiffer, R., Simon, F., Kuzmany, H. and Popov, V. N., Detailed analysis of the Raman response of n-doped double-wall carbon nanotubes, *Phys. Rev. B*, 2006, 74, 235419.

[23] Zhou, W., Xie, S., Sun, L., Tang, D., Li, Y., Liu, Z., Ci, L., Zou, X. and Wang, G., Raman scattering and thermogravimetric analysis of iodine-doped multiwall carbon nanotubes, *Appl. Phys. Lett.*, 2002, 80(14), 2553–2555.

[24] Wang, J. L., Gu, M., Zhang, X. and Song, Y., Thermal conductivity measurement of an individual fiber using a T type probe method, *J. Phys. D: Appl. Phys.*, 2009, 42, 105502.

[25] Klemens, P. G., Theory of the thermal conductivity of solids, in: Tye, R. P., ed., *Thermal Conductivity (vol. 1)*, Academic Press, London, 1969, 1–68.

[26] Dresselhaus, M. S., Jorio, A., Souza-Filho, A. G. and Saito, R., Defect characterization in graphene and carbon nanotubes using Raman spectroscopy, *Phil. Trans. R. Soc. A*, 2010, 368, 5355–5377.

[27] Hone, J., LIaguno, M. C., Nemes, N. M., Johnson, A. T., Fischer, J. E., Walters, D. A., Casavant, M. J., Schmidt, J. and Smalley, R. E., Electrical and thermal transport properties of magnetically aligned single wall carbon nanotube films, *Appl. Phys. Lett.*, 2000, 77(5), 666–668.

[28] Miao, M. H., Electrical conductivity of pure carbon nanotube yarns, *Carbon*, 2011, 49, 3755–3761.

[29] Marconnet, A. M., Panzer, M. A. and Goodson, K. E., Thermal conduction phenomena in carbon nanotubes and related nanostructured materials, *Rev. Mod. Phys.*, 2013, 85(3), 1295–1326.

[30] Sturm, J., Grosse, P. and Theiβ, W., Effective dielectric functions of alkali halide composites and their spectral representation, *Z. Phys. B-Condensed Matter*, 1991, 83, 361–365.

[31] Choi, S. U. S., Zhang, Z. G., Yu, W., Lockwood, F. E. and Grulke, E. A., Anomalous thermal conductivity enhancement in nanotube suspensions, *Appl. Phys. Lett.*, 2001, 79(14), 2252–2254.